Physics Letters B 832 (2022) 137256

Contents lists available at ScienceDirect

Physics Letters B

www.elsevier.com/locate/physletb

Hints of quasi-molecular states in ^{13}B via the study of ^{9}Li-^{4}He elastic scattering

A. Di Pietro [a,*], A.C. Shotter [b], J.P. Fernández-García [c,d], P. Figuera [a], M. Fisichella [a], A.M. Moro [c], M. Alcorta [e], M.J.G. Borge [f], T. Davinson [b], F. Ferrera [a], A.M. Laird [g], M. Lattuada [h,a], N. Soić [i], O. Tengblad [f], D. Torresi [a], M. Zadro [i]

[a] INFN, Laboratori Nazionali del Sud, via S. Sofia 62, 1-95123 Catania, Italy
[b] School of Physics and Astronomy, University of Edinburgh, JCMB, Peter Guthrie Tait Road, EH9 3FD, Edinburgh, UK
[c] Departamento de FAMN, Universidad de Sevilla, Apartado 1065, 41080 Sevilla, Spain
[d] Centro Nacional de Aceleradores, Universidad de Sevilla, Junta de Andalucía-CSIC, 41092 Sevilla, Spain
[e] TRIUMF, 4004 Wesbrook Mall, Vancouver, BC V6T 2A3, Canada
[f] Instituto de Estructura de la Materia, CSIC, Serrano 113 bis, E-28006 Madrid, Spain
[g] School of Physics and Astronomy, University of York, York, UK
[h] Dipartamento di Fisica e Astronomia, Universitá di Catania, via S. Sofia 64, I-95123 Catania, Italy
[i] Ruđer Bošković Institute, Bijenička cesta, 54 HR-10000 Zagreb, Croatia

ARTICLE INFO

Article history:
Received 2 March 2022
Received in revised form 2 June 2022
Accepted 17 June 2022
Available online 21 June 2022
Editor: B. Blank

Keywords:
Radioactive beam
Elastic scattering
Clusters

ABSTRACT

This paper reports on elastic scattering excitation functions for the reaction ^{9}Li+^{4}He measured at backward angles in the centre of mass energy range 5 MeV $\leq E_{c.m.} \leq$ 9.5 MeV, with the aim of investigating the possible existence of molecular resonances which have been predicted to exist in the case of neutron-rich B-isotopes. Due to the short lifetime of ^{9}Li, the experiment necessitated the use of inverse kinematics on a gaseous ^{4}He target. The Thick Target Inverse Kinematics technique was used which allowed for the measurement of the full excitation function in a single ^{9}Li run. Broad resonances were observed in the excitation region for ^{13}B 15 MeV $\leq E_x \leq$20 MeV. To understand the nature of such broad structures, various theoretical attempts are reported concerning possible reaction mechanisms for this neutron rich reaction. The most promising approach to interpret the data is within the orbiting reaction scenario.

1. Introduction

When two nuclei interact in their peripheral surface region, a variety of phenomena may result: elastic and inelastic scattering, pick up, transfer or breakup of one or both of the participating nuclei. Often it is assumed that such phenomena are governed by a transition matrix element linking the entrance channel quantum state, to the final quantum state by a one-step perturbing potential. However, it has been long recognised that for some reactions this one-step transition could not explain all experimental features, in particular the differential cross sections at large scattering angles. One possible explanation is that when two reacting nuclei first interact in the peripheral region, they begin to rotate about each other, and it is only after rotating by a finite angle that they make a transition into the final channel. This so-called orbiting phenomenon was extensively studied over many years by investigating mainly reactions with stable nuclei [1–10].

It is now well established that neutron-rich light nuclei have a larger extension of the matter density radius than stable nuclei. As more neutrons are added to an isotope, the binding of the neutrons decreases resulting in a greater extension of the neutron outer regions, and, in some extreme cases, a neutron-halo (n-halo) appears. It has been shown that, in the case of collisions induced by n-halo nuclei, the reaction dynamics exhibits a variety of effects connected to the extension of the neutron wave function. Indeed, the extension of the halo, the low binding energy and the large dipole strength above threshold, affects various reaction processes, such as elastic scattering, breakup and transfer [11–19]. Therefore, this raises an important question: does a more extensive neutron tail lead to a greater importance of orbiting and, if so, what implications would this have for the final reaction outcomes? This is an important question, since such exotic isotopes are thought to

* Corresponding author.
E-mail address: dipietro@lns.infn.it (A. Di Pietro).

https://doi.org/10.1016/j.physletb.2022.137256

be produced in various dynamic astrophysical events, and the reactions between them are one of the most important factors which determine the evolutionary path.

This letter reports on a study concerning the ^{4}He elastic scattering reaction mechanism from ^{9}Li, which is a neutron-rich nucleus. A possible hint of the underlying mechanisms for the ^{9}Li+^{4}He reaction may be found in the theoretical results of Kanada En'yo et al. [20]. These calculations clearly indicate that the entrance channel of the reaction ^{9}Li+^{4}He would be influenced by the rotational band structure of ^{13}B. Further, the mass density plots of the rotational bands that could be excited by the ^{9}Li+^{4}He channel, show that the density profile of some states could be an indication that possible molecular systems are formed between the ^{9}Li and ^{4}He ions rather than a symmetric fused compound nucleus. A pictorial representation of this is that at particular reaction energies, and for a range of impact parameters (i.e. angular momentum), the helium ion is temporarily captured by the weak attraction of the extended neutron tail of ^{9}Li and begins to rotate about it. However, this transient quasi-molecular state is unstable and will either evolve by ejecting the ^{4}He back into the elastic entrance channel, or excite inelastic degrees of freedom leading to other reaction channels. This will mean that the elastic cross section will exhibit broad energy resonances due to the transient nature of these quasi-molecular states. In addition, the differential cross section at backward angles is likely to be enhanced due to the orbiting of the ^{4}He ion about the ^{9}Li ion.

Experimental reaction investigations involving such short-lived isotopes are challenging due to the difficulty of producing beams of sufficient intensity. TRIUMF is one of the foremost laboratories in the world to produce such beams by the ISOL method. Nevertheless, the beam intensities are rarely sufficient to study more than the elastic or one or two high yield inelastic channels. In this paper we report a first experiment to study the elastic reaction ^{9}Li+^{4}He, specifically to investigate the possibility that transient orbiting could be influencing this channel.

2. Experiment

The experiment was performed at the TRIUMF laboratory (Canada) using a 32 MeV ^{9}Li beam delivered by ISAC-II impinging on a ^{4}He gas target. The Thick Target Inverse Kinematic (TTIK) technique was adopted for the experiment [21]. When passing through the ^{4}He gas target the beam loses energy, elastic scattering may occur in a continuous range of energies starting from the initial beam energy entering the target down to zero. Indeed, the ^{9}Li beam is stopped in the gas before reaching the detectors, while the recoiling α particles, owing to the lower stopping power, are detected. In the present experiment, the target consisted of the TUDA chamber (see Fig. 1) filled with isotopically pure ^{4}He gas at pressure of 650 Torr, enough to stop the beam before reaching the zero degree detector. The temperature of the gas was continuously measured using a thermocouple. A $\phi = 20$ mm Kapton window $\approx$ 12 µm thick was used to separate the gas-filled chamber from the high vacuum beam line. During the experiment, the gas pressure was continuously monitored, and the gas was replaced several times. α-particles from elastic scattering were detected and discriminated from other reaction processes using Time of Flight (ToF) techniques. The detected α-particle energy depends on the reaction process that has produced it, as well as on the position in the target where the reaction has occurred. If the target is extended enough, the ToF measurement allows discrimination of elastic scattering from other reaction events, for example, inelastic scattering.

The detection system consisted of three telescopes each made of 50×50 mm^2, 50 µm thick silicon detector segmented into four-quadrants as ΔE and a 50×50 mm^2, 1500 µm thick single PAD silicon as residual energy detector. A sketch of the experimental set-up is shown in Fig. 1. One of the telescopes, T1, was centred at $\theta_{lab} = 0°$, and telescope T2 was adjacent to T1. The four quadrants of T1 were covering the same scattering angles. Telescopes T1 and T2 were placed downstream of the TUDA chamber, at approximately 1400 mm from the Kapton window. A third telescope, T3, was positioned closer to the entrance window, at about 600 mm, and angled at 45° with respect to the beam axis. In this way, although in T3 the excitation function was not measured in the full excitation energy range as for T1 and T2, it provided a broader angular distribution measurement for the highest excitation energy events. For telescopes T2 and T3 the quadrants up and down of each ΔE detector were at the same scattering angles. To measure ToF, a microchannel plate (MCP) detector [22] was placed under vacuum, upstream of the Kapton window; it gave a signal whenever a ^{9}Li beam particle entered into the chamber, hence, it was also used for the cross-section normalisation. The beam intensity was kept to $\simeq 5\times10^5$ pps to avoid pile-up events. The MCP efficiency for 32 MeV ^{9}Li beam was measured to be $\varepsilon = 99\%$. The detectors around $\theta_{lab} = 0°$, besides αs and protons produced in the reaction, were detecting also βs and β-delayed αs coming from the radioactive decay of the ^{9}Li beam. This background was very large in detector T1 since the beam was stopped in the gas a few cm before reaching the detector. This necessitated the introduction of an energy threshold for accepting the detected α particles of ∼5 MeV.

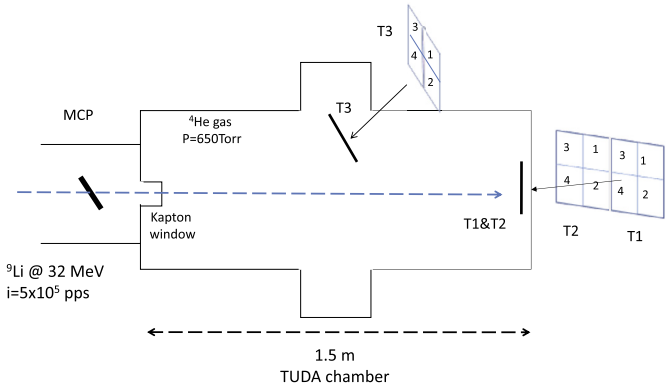

Fig. 1. Sketch of the experimental set-up. See text for details.

Events of interest in telescopes T2 were also selected with an energy threshold of ∼ 4 MeV. In fact, below this energy, helium and hydrogen particles which stop in the ΔE detector cannot be discriminated in time. This can be seen in Fig. 2 which shows the ToF *vs* ΔE spectrum for detector T2. The detected α particles in detector T3, due to its position in the chamber, have an energy above 15 MeV. This means for this detector no events at c.m. energies lower than ∼ 8 MeV could be detected.

In Fig. 2 besides elastic scattering, inelastic scattering events can be observed just above the elastic locus. These events can be discriminated with proper gating. For α-particles stopping in the ΔE detector, the selection of events was undertaken by putting gates on the elastic locus of the ΔE *vs* ToF spectrum (see Fig. 2), with the condition that no particle was detected on the residual energy detector E; whereas, for the high energy events, punching through the ΔE, gates on both E *vs* ToF, and ΔE *vs* E, were set. Residual background coming from the radioactive decay of the beam was subtracted by shifting the gates on the ΔE *vs* ToF in a different time-energy region where only time-uncorrelated events occurred. For the events punching through the ΔE detectors, the total energy ($\Delta E+E_{res}$) was reconstructed on an event by event basis, correcting for the energy loss in the dead-layers of the detectors and in the gas volume in between the two detectors of the telescope.

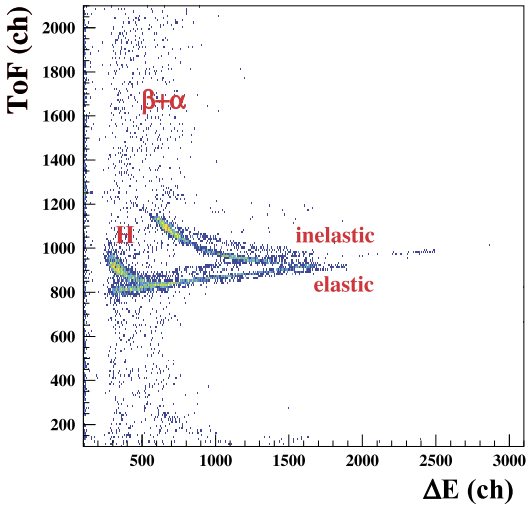

Fig. 2. ToF *vs* ΔE energy spectrum for one quadrant of telescope T2. The ToF corresponds to the sum of the time of flight of the beam before interacting with the target plus the time of flight of the recoiling particles. The ToF start signal is given by the Si detectors while the stop is given by the delayed MCP signal. α-particles coming from elastic and inelastic events are clearly distinguished. Beta and alphas background events, uncorrelated in time, coming from the ^{9}Li radioactive decay can be observed. The threshold energy of 4 MeV corresponds to channel $\sim$ 700.

Centre of mass energy spectra, for elastically scattered α-particles, have been obtained from the energy deposited in the detectors, information of the detector geometry and the stopping power of the ^{4}He gas for both the beam and the αs. Knowledge of stopping power is crucial for this type of measurements, as shown in [23], not only to deduce the centre of mass energy but also the cross-section. For this reason the stopping power of helium gas for Li was measured using the stable ^{7}Li isotope [24]. A very good agreement was obtained in this case between the measured stopping power and the one calculated by SRIM [25]. The electronic stopping power depends only on the atomic features of the ions. The scaling of different isotopes requires only the change in velocity arising from the difference in mass, which can be calculated. Therefore, in the analysis, the energy loss of ^{9}Li, as well as the one for αs on Helium, was calculated using SRIM. Indeed, it was verified, by changing gas pressure, that the measured energy loss of ^{9}Li through various target thicknesses corresponded to the calculated one.

Since the TTIK technique involves a complex relationship between the measured quantities (energies and position of the detected αs) and the reconstructed ones (c.m. energy and scattering c.m. angle), a Monte Carlo simulation was undertaken to quantify the details of the relationship. Simulations included energy and angular straggling for the beam and the recoiling α-particles. An example of such a simulation, regarding the angular distribution, is shown in Fig. 3. Here, simulation of elastic events were generated corresponding to ^{13}B 19.5 MeV excitation, and with c.m. angular distribution corresponding to the Legendre polynomial $|P_{\ell}(\cos\theta)|^2$, with $\ell = 7$. Events were then allowed to be intercepted by the detector. The number of events in each detector were recorded. These numbers were then associated with the mean scattering angle of each of the fired detector quadrants and the corresponding event location within the gas. The full line shows the $|P_{\ell=7}(\cos\theta)|^2$ Legendre polynomial and the points, the probability an event will be recorded in the detector quadrant mean angle as given by the Monte Carlo. As one can see from the figure there is only a very small difference between the analytical form and the results of the simulations for the smallest measured angles. These outcomes give confidence that the experimental results are not affected by the complexity of the experimental technique adopted.

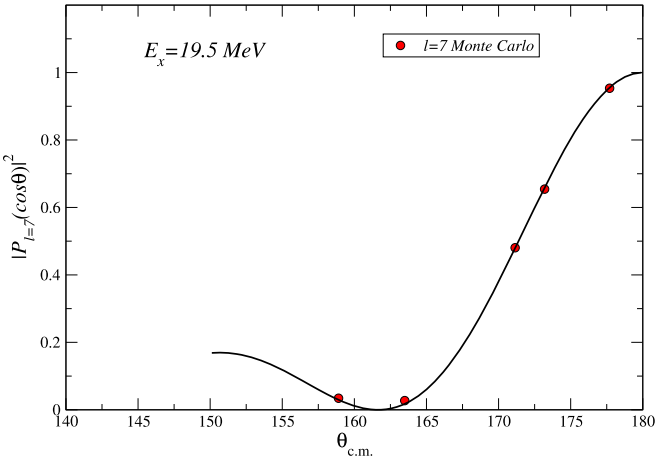

Fig. 3. (Symbols) Monte Carlo simulation results for a $\ell = 7$ Legendre polynomial in the case of the detector geometry corresponding to an excitation energy $E_x = 19.5$ MeV. The symbols correspond to the mean-probability of detection at the mean angle of each detector. (full line) $|P_{\ell=7}(\cos\theta)|^2$ Legendre polynomial. See text for details.

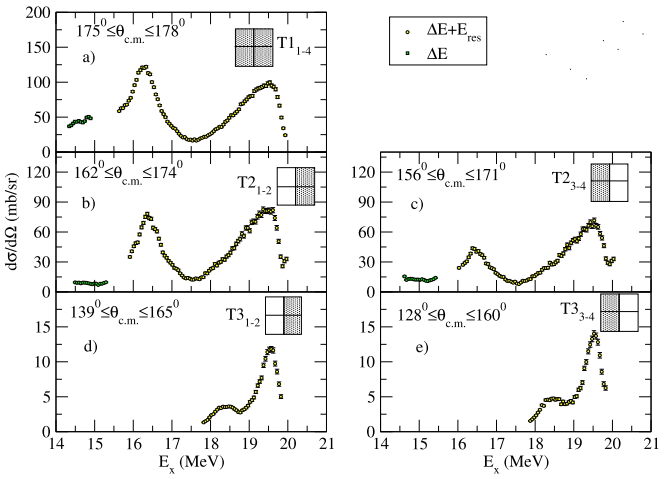

Fig. 4. ^{13}B excitation functions. Each plot represents the excitation function in the angular region specified. Angles change with energy, the smallest angle of each plot corresponds to the minimum energy and the largest angle to the maximum energy (see text for details). In the plot are also indicated the detectors used to extract the associated excitation function.

3. Results

The ^{13}B excitation energy spectrum was obtained from the $E_{c.m.}$ spectrum by adding the two-body $Q_{val} = 10.82$ MeV. In Fig. 4 the excitation functions at various detector scattering angles are shown. Each angular range covered by a detector corresponds to the detection module sketched in Fig. 1 and Fig. 4. Using the TTIK technique means that a particular detector records events for scattering angles which depends on the location of the events within the gas, that in turn determines the associated excitation energy of the events. Hence, each energy bin in Fig. 4 corresponds to a bin in angle which, in turn, depends on the detector geometry. In each plot the minimum and maximum angles reported correspond to the smallest and largest excitation energy measured, respectively. The Monte Carlo simulations performed were used to deduce detection efficiency as well as the c.m. energy resolution, which varies from $\sim$40 keV to $\sim$100 keV FWHM, and the c.m. angular resolution, which varies from $\sim$0.1° to $\sim$3°, depending on energy and detector. In Fig. 4 the excitation function at the most backward angles (telescopes T1 and T2) shows two broad peaks, centred at ^{13}B excitation energy of $E_x \approx 16.3$ MeV and $E_x \approx 19.5$

MeV with strong angular dependence. The excitation function of telescope T3, shows the appearance of a possible third peak at $E_x \approx 18.4$ MeV.

4. Theoretical interpretation

Nuclei participating in reactions are traditionally either considered to completely merge into a slowly evolving compound system, or directly interact only in their peripheral regions. If a compound system is formed, this can lead to narrow resonances for σ *vs* E, while the direct processes lead to more smoothly varying cross sections. R-matrix calculations have been particularly useful to help identifying the resonance parameters associated with measured resonances in the elastic channel excitation function. As discussed below, the R-matrix method has been used in an attempt to interpret the experimental data. For reasons that will be discussed, this has not been very successful. Alternative to compound nucleus resonances, orbiting or shape resonances may occur. In order to investigate this possibility a simplified orbital model is introduced which, although simple, has the merit of needing few parameters, which can, in addition, be related to known information. Using the information derived from the orbital model, optical model calculations were performed, confirming the results of the simplified model. In what follows, the R-matrix together with the seemingly more successful orbital model and optical model calculations will be reported.

4.1. R-matrix

In order to obtain spectroscopic information on the structures observed in the excitation functions, R-matrix analysis is widely adopted. The R-matrix theory is an accurate theory and its application is not in its general formulations limited to reactions that proceed by compound nucleus formation. In principle it can be used to describe all types of reaction phenomena where either "strong absorption or moderate absorption [26]" occur. Therefore, R-matrix can describe nuclear reactions in which nuclei do not form a compound nucleus but directly scatter each other with or without a change in their internal structures. Moreover, it can be applied also to the case of overlapping levels, i.e. the compound nucleus continuum. However, there are underlying hypothesis and/or approximations that are necessary when the theory is applied to a specific process [26,27]. Therefore, care must be taken when performing calculations with the available R-matrix codes.

In the present experiment the ^{9}Li+^{4}He excitation function was measured in a ^{13}B excitation energy region where, n ($S_n = 4.88$ MeV), $2n$ ($S_{2n} = 8.2$ MeV), α ($S_\alpha = 10.82$ MeV), t ($S_t = 10.995$ MeV), p ($S_p = 15.80$ MeV) and d ($S_d = 16.75$ MeV) channels are open.

No information about ^{13}B states in the excitation region explored here is available in the literature, nor can be inferred by looking at isobaric analogue states in neighbours nuclei because they would be at very high excitation energy. Moreover, none of the open competing outgoing channels, listed above, have been measured experimentally as they involve reactions with radioactive beams.

A further difficulty comes from the examination of the extracted excitation functions, where only three broad peaks are observed with the possible contribution of a fourth peak at an excitation energy ~18.9 MeV that disappears at smaller angles (Figs. 4d and 4e).

The R-matrix code AZURE2 [27] was used for the present analysis. In AZURE2 the reaction is assumed to proceed through the population of a set of compound nucleus states which, in turn, decay into one of the open reaction channels. The underlying hypothesis in the present analysis is, hence, that the observed peaks

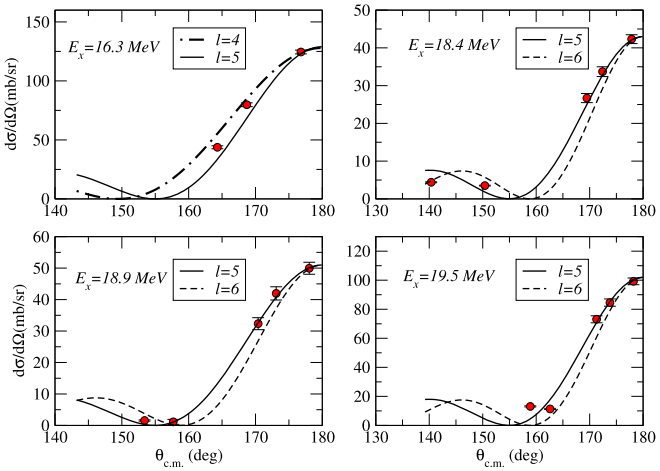

Fig. 5. (Symbols) angular distribution at four excitation energies. (dot-dashed line) $\ell = 4$, (full line) $\ell = 5$, (dashed line) $\ell = 6$ Legendre polynomials normalised to the experimental cross-section at the most backward c.m. angle. See text for details.

in the excitation functions correspond to resonances of the compound nucleus ^{13}B. However, the observed resonances are very broad and smoothly varying, indicating single broad resonances rather than accumulation underlying narrow resonances. Thus, this hypothesis of compound nucleus formation may not be appropriate in the present case.

A multilevel-mulichannel R-matrix fit was performed. As possible exit channels, along with elastic scattering, the n+^{12}B and p+^{12}Be have been taken into account. In order to reduce the number of free parameters, for each J^π the lowest ℓ values were considered. To define the input parameters, the angular distributions shown in Fig. 5 were used as guidance. In this figure each point in the angular distribution was extracted by considering the cross section value at the corresponding E_x. It was verified that performing a fit of the excitation functions with multiple gaussians or lorentians did not modify the behaviour of the angular distribution. The lines in the figure represent Legendre polynomials normalised to the experimental cross-section at the most backward c.m. angle. States with $\ell = 4, 5, 6$ were included, as well as possible contributions from lower ℓ. A lengthy survey of the possible spins contributing to the excitation functions shown in Fig. 4 a, b and c was undertaken with the aim of finding the most relevant J^π contributing to the ^{13}B excitation energy spectrum. It was found that possible spins are $J^\pi = \frac{5}{2}^-$, $\frac{7}{2}^-$, $\frac{9}{2}^+$, $\frac{11}{2}^+$ and $\frac{13}{2}^-$, but other contributions cannot be ruled out. These spins were used as input parameters for the best-fit of the data. Energies and widths of the states were considered as free parameters. A separate fit was determined for each individual excitation functions of Fig. 4a, 4b and 4c. The optimised parameters of each separate fit had similar energies for the corresponding J^π but very different widths in all final channels included in the fit. Although individual fits could be made, when using the optimised parameters obtained from the fit of any one excitation function to fit the others, good fits were never achieved. So, a converged simultaneous fit of all excitation functions was not obtained, even after the many attempts that were made. This seems to demonstrate, in the present case, the limit of this approach which assumes the presence of long-lived compound nucleus states while the excitation functions shows instead very broad (i.e. short-lived) structures.

4.2. A molecular orbital rotational interpretation

For energies above the Coulomb barrier, shape resonances may occur at angular momentum $\ell \sim kR$. These resonances correspond to quasi-molecular states whose peculiarity is: large back-

scattering cross section with angular distributions characteristic of ℓ [7]. The cross-section and angular distribution observed experimentally in the present study may be an indication of the occurrence of molecular-type resonances originated from an orbiting-type phenomenon. As referred to in Sec. 1, the phenomenon of orbiting for stable reacting nuclei has been studied for some time. This phenomenon is essentially a rolling process where the reacting nuclei encounter each other at an impact parameter near the sum of their radii. After attachment and rolling, they break apart, often resulting in an enhancement of cross-section at backward angles. However, for neutron rich nuclei, this surface interaction region will be extended. So, the question arises as to whether orbiting is more prevalent for neutron rich nuclei than stable nuclei. This experiment involving ^{9}Li and ^{4}He has shown broad resonances at backward scattering angles. So, could this resonance behaviour observed in this experiment be linked to an orbiting phenomenon? The possibility that this might be so is outlined below.

For the reaction system like ^{9}Li+^{4}He, the extended low density neutron field of ^{9}Li provides a weak attraction for orbital angular momentum components of the wave function corresponding to peripheral interactions between the two ions. The simplest model to represent this physical situation is a two-step potential with a volume core potential $V_C(r)$ for $0 \leq r < r_1$ and a shallow surface potential $V_S(r)$ for $r_1 \leq r \leq R$. For this light ion system, the Coulomb potential is small, and so to a first approximation $V_C(r)$ and $V_S(r)$ are taken as constant potentials, V_C and V_S, respectively (which can be complex). In this case, it is possible to express the reaction wave-functions for r<R as combinations of spherical Hankel functions. The external wave-function will be a combination of incoming and outgoing Coulomb wave components, which are related to hypergeometric functions [28]. By matching the amplitude and slopes of wave-function components at r_1 and R, it is possible to derive an analytical expression for the scattering matrix, and so the differential cross section.

A close inspection of the results of Kanada En'yo et al. [20], indicates that the cross-section for the reaction ^{9}Li+ ^{4}He at a c.m. energy corresponding to 19.5 MeV excitation energy in ^{13}B, could be associated with a molecular resonance with angular momentum $\ell = 5\hbar$, and with $r_1 = 3.4$ fm and R=5.1 fm. Using these values of ℓ, r_1, R and the c.m. energy, it was found that the intensity of the wave function within the radial shell $r_1 \leq r \leq R$ varies rapidly with the value of V_S, reaching a maximum when V_S = -13.16 MeV. This reaction condition also produced resonance peaks corresponding to ^{13}B excitation energies of 15.8 and 13.2 MeV, with values of angular momentum $4\hbar$ and $3\hbar$ respectively. For this value of V_S, Fig. 6 full line, shows the calculated cross section at the average angles corresponding to the data of Fig. 4, where the most appropriate V_C was found to be $V_C = -(148+i\times33)$ MeV. This value of the real component of the potential seems consistent with previous investigations [29]. A point of note, is that the magnitudes of the resonant peaks of Fig. 6 were found to strongly depend on the value of V_C, but the resonance energy positions were insensitive.

This simplified approach (identified here as TRM, Transient Rotational Model) to investigate the reaction mechanism yields an analytical expression for the scattering matrix, so it is straightforward to explore its structure over the complex angular momentum plane. It has been known for some time that the scattering amplitude for a reaction can be represented by a closed path integral in the complex angular momentum plane (often regarded as a background contribution), together with a sum of residuals of singularity poles associated with any resonances [30]. For the parameters specified above, the complex plane profiles of the scattering matrix at the resonances are shown in Fig. 7. For each resonance there is a clear singularity pole. It can be shown that the angular momentum imaginary values of the poles are related to the decay-time of

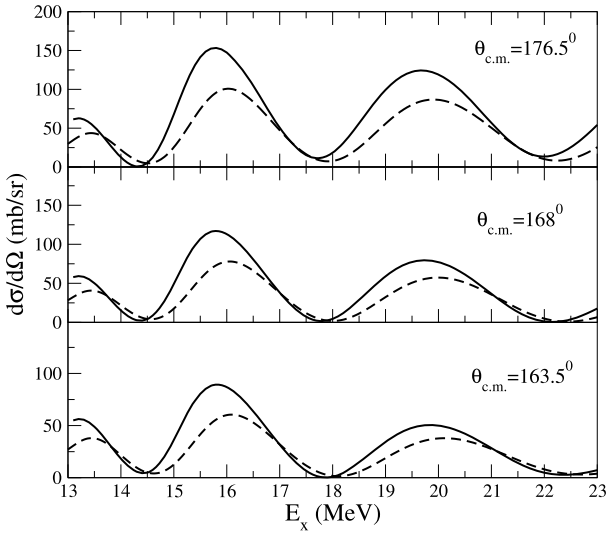

Fig. 6. (Full line) The analytical model (TRM) predictions of the differential cross sections for the average angles of the experimental data. (Dashed line) Optical model calculations with the two-step potential of the TRM. See text for details.

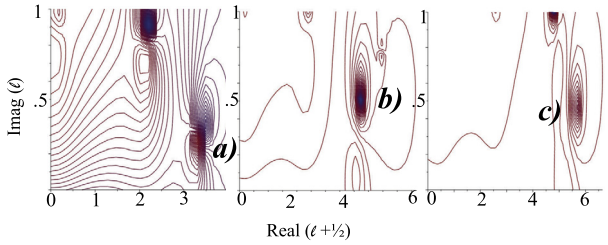

Fig. 7. Angular momentum plane intensity profiles of the modulus of the scattering matrix at the resonant energies shown in Fig. 6. a) corresponds to a pole at $E_x = 13.2$ MeV, $\ell = 3\hbar$; b), corresponds to a pole at $E_x = 15.8$ MeV, $\ell = 4\hbar$; c), corresponds to a pole at $E_x = 19.5$ MeV, $\ell = 5\hbar$.

the resonances, so yielding a lifetime of 1.94×10^{-22} s for resonance b), and 1.68×10^{-22} s for resonance c). For these lifetimes, and using a semiclassical treatment of the rotating flux within the V_S shell, the rotating ^{9}Li+ ^{4}He system breaks apart before a half rotation is completed.

Clearly, there is not a complete agreement between the analytical and experimental results, see Figs. 4 and 6. Due to the simplifications of the model, this is not unexpected. A close inspection of the measured resonance structure in the region of 18 to 20 MeV, Fig. 4, indicates that there are more structures than a single resonance. One possibility is that the single orbital resonance associated with the TRM is energy split due to a spin-orbit interaction potential, $V_{so}\ell \cdot s$, in the surface region. For $\ell = 5$, this will split the single resonance into four components. In fact, it is possible to identify at least three components 18.4, 18.9 and 19.5 MeV, which seem to follow an $\ell = 5$ angular distribution, Fig. 5. The fourth component may be an unresolved part of one of these three identified components. The analytical model shows that the $\ell = 5$ resonance will be spread by 1.1 MeV when a spin-orbit potential, with $V_{so} = 0.12$ MeV, is combined with the shell potential -13.16 MeV. This spin-orbit potential is taken as a constant in the surface region rather than a function of radius; nevertheless, this value of 0.12 MeV is reasonably consistent with other analyses involving spin-orbit potentials for light mass systems (e.g. [31]). The addition of this small surface spin-orbit potential has an interesting influence on the position of the four resonant pole components in the complex angular momentum plane. The real part of the poles only varies by a few percent, but the imaginary parts vary by up

Table 1
Optical potential parameters of the real and imaginary part of the optical potential of the core C and surface S potentials. The potential depths are in MeV, radii and diffuseness in fm. See text for details.

V_C	R_C	a_C	V_S	R_S	a_S
122.44	4.36	0.03	7.24	7.11	0.50
W_C	R_{WC}	a_{WC}	W_S	R_{WS}	a_{WS}
33	3.4	0.05	1.11	4.38	0.01

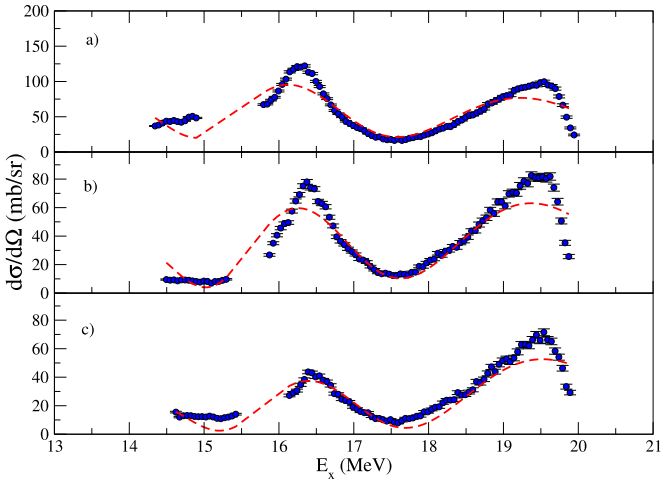

Fig. 8. Experimental (symbols) and calculated excitation function with an optical model fit (dashed line). a) telescope $T1_{1-4}$; b) telescope $T2_{1-2}$; c) telescope $T2_{3-4}$.

to 40%, which will influence the energy widths and decay times of the different resonant components.

An important feature of such a simple model is that it provides physical insight into the reaction mechanism such as the concentration of wave intensity within the surface region and its temporal decay. It also provides guidance to the parameters that can be used in optical model codes such as FRESCO [32].

As a cross-check between the TRM analytical results and the optical model (OM), the FRESCO code was run with the same two potentials as for the TRM; the results are shown in Fig. 6, as full lines for the TRM and dashed lines for the OM model calculations. As one can see from the figure, the OM calculations produce similar results as TRM. Three peaks are observed in the region of interest of the excitation function, peaked at approximately the same excitation energy. However, in Fig. 6 it can be seen that the cross section magnitudes and peak positions do not quite agree. This may be due to the TRM model using a constant potential within the potential wells, whereas the full optical model code will take account of the varying Coulomb potential within the wells, which will presumably suppress the cross sections and rises the energy of the peaks.

Guided by the above results, a OM search was then undertaken to use the two potential concept, and to allow the parameters to vary until a best fit was achieved to the experimental data. The calculations used two squared Woods-Saxon potentials, real and imaginary, both for the core and the surface. The fit was performed having as free parameters depth, radius and diffuseness of the real part of both, the core and the surface potential. A fit was attempted also by varying the parameters of the imaginary part of the core and surface potentials, leading to a poorer result. The parameters of the best fit are listed in Table 1. Fig. 8 shows the results of the OM fit. The agreement between the OM fit and the data is rather satisfactory. The potential parameters are not too different than the ones of the TRM, only the surface is more extended.

In addition to the above investigation using FRESCO, extensive searches were made using other types of potentials. For example, starting with a single Woods-Saxon and a spin-orbit potential, with parameters similar to those reported by Taylor et al. [31] for the ^{9}Be+ ^{4}He elastic reaction, an investigation was undertaken as to whether, for given partial waves, there are resonant peaks in the elastic scattering excitation function in the region of interest. Initially, the potential was assumed to be purely real, with the absorptive terms included in a second step. Indeed, the calculations showed that the elastic cross-section exhibit strong peaks for selected J^{π} at the $E_{c.m.}$ energy of interest, with various widths. The choice of the spin-orbit potential changed the energy position of the peaks. When adding the imaginary potential, sharp peaks were fully absorbed while the broader structures survived, provided the imaginary potential did not extend up to the surface of the nucleus. At the conclusion of these searches, a fit better than shown in Fig. 8 could not be found.

Finally, it is interesting to note the basic difference between these two types of optical model calculations. The more successful one (Table 1), separates the potential into two separate and distinct regions, whereas the conventional approach (e.g. [31]) just considers the surface as the diffused part of a single central core. So this result seems to highlight the distinct nature of the surface tail from the central potential core.

5. Summary and conclusions

The main objective of this experiment was to investigate the possible existence of molecular resonances which have been predicted to exist in the case of n-rich B-isotopes [20]. The research discussed in this paper was, in fact, inspired by the work of Kanada En'yo et al. [20]. This indicated the possibility, at high excitation energies, that the ^{13}B nucleus could exhibit molecular type resonances with ^{4}He and ^{9}Li clusters coupled in rotational states. Although this study indicated such states would be bound, they would in reality be above the helium plus lithium threshold. So if the structures are still preserved they would be quite energy broadened. Therefore, the entrance channel of helium plus lithium reaction may be influenced by these rotational states, which nevertheless would be quite short lived.

One of the most direct ways to investigate experimentally this theoretical result is study of the ^{4}He+^{9}Li elastic channel. However, this can only be undertaken with a radioactive ^{9}Li beam which is unstable and so only can be produced with limited intensities. The experiment reported in this paper involved study of ^{9}Li+^{4}He elastic scattering using an extended gas target, so the reaction could be studied over a range of bombarding energies initiated by one beam entrance energy into the gas cell, thus reducing the beam-time. The disadvantage of this method is that it is challenging to uncouple events at different reaction energies within the gas and their corresponding angular distributions. Nevertheless, using Monte Carlo simulations to unfold the experimental data, excitation functions over 14.5 to 20 MeV energy, and for various scattering angle ranges have been obtained. The excitation functions at a range of angles, show peak cross section values at 16.3, 18.4 and 19.5 MeV.

Three approaches were used in attempts to interpret data. The first approach concerned the use of R-matrix analysis to see if a set of compound nucleus resonances could consistently reproduce the observed data. This did not seem to be the case. It was found that, while it was possible to fit the experimental data at particular scattering angles with a set of resonance parameters, these parameters were not unique and substantially varied for different angles, i.e. a universal set of resonance parameters could not be found to fit all angles. The second approach was to follow up the possibility that the entrance channel, in the energy range

explored, is influenced, to some degree, by molecular type resonances, as indicated by the work of Kanada En'yo et al. [20]. To this end, a simplified molecular rotational reaction model was developed. The various parameters of the model were deduced from Kanada En'yo et al. [20]. It was found that the model predicts reasonably close values to the energies and cross section magnitudes of the 16.3 and 19.5 MeV resonances. Finally, the last attempt to interpret the data was to use an optical model with various interaction potentials deduced from other similar elastic reactions (e.g. ^{9}Be+^{4}He).

At the conclusion of these three approaches, it was considered that the interpretation that best describes the data, in this entrance channel energy range, is that to some degree molecular type resonances are responsible. However, this can only be a tentative conclusion, since the measured angular distributions are quite limited. To follow up this work, it would be most interesting to study the reaction with solid helium targets [33] and ref. therein, so complete angular distributions could be measured at the resonance peaks observed in this experiment. Moreover, it would be important to investigate if, for neutron rich nuclei, where the low-density neutron tail weakly interacts with the incoming projectile, the orbiting reaction scenario is a common feature, and if it is more prevalent for these nuclei than for stable ones.

Declaration of competing interest

The authors declare that they have no known competing financial interests or personal relationships that could have appeared to influence the work reported in this paper.

Data availability

Data will be made available on request.

Acknowledgements

This work was supported by INFN and partially supported by the Ministry of Science, Innovation and Universities of Spain, through the projects PGC2018-096994-B-C21, PID2019-104390GB-I00, PID2020-114687GB-I00 and by the Consejería de Economía, Conocimiento, Empresas y Universidad, Junta de Andalucía (Spain) through the project P20_01247.

References

[1] S. Bosanac, Contribution of orbiting to differential cross sections, Phys. Rev. A 19 (1979) 125–133, https://doi.org/10.1103/PhysRevA.19.125.
[2] P. Braun-Munzinger, J. Barrette, Dynamical aspects of large angle heavy-ion scattering, Phys. Rep. 87 (5) (1982) 209–258.
[3] S. Landowne, Structure in backward-angle excitation functions for strongly absorbed particles, Phys. Rev. Lett. 42 (10) (1979) 633.
[4] R. Fuller, Quasimolecular state and Regge poles, Nucl. Phys. A 216 (1) (1973) 199–216.
[5] T. Tamura, H. Wolter, Regge description of optical-model scattering, Phys. Rev. C 6 (6) (1972) 1976.
[6] A. Arima, G. Scharff-Goldhaber, K. McVoy, Possible quasi-molecular rotational bands in sd-shell nuclei, Phys. Lett. B 40 (1) (1972) 7–10.
[7] K.W. McVoy, Regge poles and strong absorption in heavy-ion and α-nucleus scattering, Phys. Rev. C 3 (1971) 1104–1117, https://doi.org/10.1103/PhysRevC.3.1104.
[8] D. Sokolovski, A. Msezane, Z. Felfli, S. Ovchinnikov, J. Macek, What can one do with Regge poles?, in: The Application of Accelerators in Research and Industry, Nucl. Instrum. Methods B 261 (1) (2007) 133–137, https://doi.org/10.1016/j.nimb.2007.04.057.
[9] W. Friedman, K. McVoy, M. Nemes, A resonant interpretation of gross structure in 12C+ 12C and16O+ 16O inelastic scattering, Phys. Lett. B 87 (3) (1979) 179–182.
[10] A. Cowley, G. Heymann, Regge pole analysis of the elastic scattering of α-particles from 16O, Nucl. Phys. A 146 (2) (1970) 465–476.
[11] A. Di Pietro, P. Figuera, F. Amorini, C. Angulo, G. Cardella, S. Cherubini, T. Davinson, D. Leanza, J. Lu, H. Mahmud, M. Milin, A. Musumarra, A. Ninane, M. Papa, M.G. Pellegriti, R. Raabe, F. Rizzo, C. Ruiz, A.C. Shotter, N. Soić, S. Tudisco, L. Weissman, Reactions induced by the halo nucleus ^{6}He at energies around the Coulomb barrier, Phys. Rev. C 69 (2004) 044613, https://doi.org/10.1103/PhysRevC.69.044613.
[12] A. Sánchez-Benítez, D. Escrig, M. Álvarez, M. Andrés, C. Angulo, M. Borge, J. Cabrera, S. Cherubini, P. Demaret, J. Espino, P. Figuera, M. Freer, J. García-Ramos, J. Gómez-Camacho, M. Gulino, O. Kakuee, I. Martel, C. Metelko, A. Moro, F. Pérez-Bernal, J. Rahighi, K. Rusek, D. Smirnov, O. Tengblad, P. Van Duppen, V. Ziman, Study of the elastic scattering of ^{6}He on ^{208}Pb at energies around the Coulomb barrier, Nucl. Phys. A 803 (1) (2008) 30–45, https://doi.org/10.1016/j.nuclphysa.2008.01.030.
[13] A. Di Pietro, G. Randisi, V. Scuderi, L. Acosta, F. Amorini, M.J.G. Borge, P. Figuera, M. Fisichella, L.M. Fraile, J. Gomez-Camacho, H. Jeppesen, M. Lattuada, I. Martel, M. Milin, A. Musumarra, M. Papa, M.G. Pellegriti, F. Perez-Bernal, R. Raabe, F. Rizzo, D. Santonocito, G. Scalia, O. Tengblad, D. Torresi, A.M. Vidal, D. Voulot, F. Wenander, M. Zadro.
[14] A. Di Pietro, V. Scuderi, A.M. Moro, L. Acosta, F. Amorini, M.J.G. Borge, P. Figuera, M. Fisichella, L.M. Fraile, J. Gomez-Camacho, H. Jeppesen, M. Lattuada, I. Martel, M. Milin, A. Musumarra, M. Papa, M.G. Pellegriti, F. Perez-Bernal, R. Raabe, G. Randisi, F. Rizzo, G. Scalia, O. Tengblad, D. Torresi, A.M. Vidal, D. Voulot, F. Wenander, M. Zadro.
[15] M. Cubero, J.P. Fernández-García, M. Rodríguez-Gallardo, L. Acosta, M. Alcorta, M.A.G. Alvarez, M.J.G. Borge, L. Buchmann, C.A. Diget, H.A. Falou, B.R. Fulton, H.O.U. Fynbo, D. Galaviz, J. Gómez-Camacho, R. Kanungo, J.A. Lay, M. Madurga, I. Martel, A.M. Moro, I. Mukha, T. Nilsson, A.M. Sánchez-Benítez, A. Shotter, O. Tengblad, P. Walden, Do halo nuclei follow Rutherford elastic scattering at energies below the barrier? The case of ^{11}Li, Phys. Rev. Lett. 109 (2012) 262701, https://doi.org/10.1103/PhysRevLett.109.262701.
[16] J.P. Fernández-García, M. Cubero, M. Rodríguez-Gallardo, L. Acosta, M. Alcorta, M.A.G. Alvarez, M.J.G. Borge, L. Buchmann, C.A. Diget, H.A. Falou, B.R. Fulton, H.O.U. Fynbo, D. Galaviz, J. Gómez-Camacho, R. Kanungo, J.A. Lay, M. Madurga, I. Martel, A.M. Moro, I. Mukha, T. Nilsson, A.M. Sánchez-Benítez, A. Shotter, O. Tengblad, P. Walden, ^{11}Li breakup on ^{208}Pb at energies around the Coulomb barrier, Phys. Rev. Lett. 110 (2013) 142701, https://doi.org/10.1103/PhysRevLett.110.142701.
[17] V. Pesudo, M.J.G. Borge, A.M. Moro, J.A. Lay, E. Nácher, J. Gómez-Camacho, O. Tengblad, L. Acosta, M. Alcorta, M.A.G. Alvarez, C. Andreoiu, P.C. Bender, R. Braid, M. Cubero, A. Di Pietro, J.P. Fernández-García, P. Figuera, M. Fisichella, B.R. Fulton, A.B. Garnsworthy, G. Hackman, U. Hager, O.S. Kirsebom, K. Kuhn, M. Lattuada, G. Marquínez-Durán, I. Martel, D. Miller, M. Moukaddam, P.D. O'-Malley, A. Perea, M.M. Rajabali, A.M. Sánchez-Benítez, F. Sarazin, V. Scuderi, C.E. Svensson, C. Unsworth, Z.M. Wang, Scattering of the halo nucleus ^{11}Be on ^{197}Au at energies around the Coulomb barrier, Phys. Rev. Lett. 118 (2017) 152502, https://doi.org/10.1103/PhysRevLett.118.152502.
[18] A. Di Pietro, A. Moro, J. Lei, R. de Diego, Insights into the dynamics of breakup of the halo nucleus ^{11}Be on a ^{64}Zn target, Phys. Lett. B 798 (2019) 134954, https://doi.org/10.1016/j.physletb.2019.134954.
[19] J.P. Fernández-García, A. Di Pietro, P. Figuera, J. Gómez-Camacho, M. Lattuada, J. Lei, A.M. Moro, M. Rodríguez-Gallardo, V. Scuderi, Breakup mechanisms in the ^{6}He +^{64} Zn reaction at near-barrier energies, Phys. Rev. C 99 (2019) 054605, https://doi.org/10.1103/PhysRevC.99.054605.
[20] Y. Kanada-En'yo, Y. Kawanami, Y. Taniguchi, M. Kimura, Cluster states in 13B, Prog. Theor. Phys. 120 (5) (2008) 917–935, https://doi.org/10.1143/PTP.120.917.
[21] V.Z. Goldberg, G.V. Rogachev, W.H. Trzaska, J.J. Kolata, A. Andreyev, C. Angulo, M.J.G. Borge, S. Cherubini, G. Chubarian, G. Crowley, P. Van Duppen, M. Gorska, M. Gulino, M. Huyse, P. Jesinger, K.-M. Källman, M. Lattuada, T. Lönnroth, M. Mutterer, R. Raabe, S. Romano, M.V. Rozhkov, B.B. Skorodumov, C. Spitaleri, O. Tengblad, A. Tumino, Investigation of the α-cluster structure of ^{22}Ne and ^{22}Mg, Phys. Rev. C 69 (2004) 024602, https://doi.org/10.1103/PhysRevC.69.024602.
[22] A. Musumarra, P. Figuera, F. De Luca, A. Di Pietro, P. Finocchiaro, M. Fisichella, M. Lattuada, A. Pakou, M. Pellegriti, G. Randisi, G. Scalia, C. Scirè, S. Scirè, V. Scuderi, D. Torresi, M. Zadro, Measuring total reaction cross-sections at energies near the Coulomb barrier by the active target method, Nucl. Instrum. Methods A 612 (2) (2010) 399–406, https://doi.org/10.1016/j.nima.2009.11.039.
[23] M. Zadro, A. Di Pietro, P. Figuera, M. Fisichella, M. Lattuada, A. Maggio, F. Pansini, M. Papa, V. Scuderi, O. Goryunov, V. Ostashko, Stopping power of helium gas for 9Be ions from 2 to 31 MeV, Nucl. Instrum. Methods Phys. Res., Sect. B, Beam Interact. Mater. Atoms 259 (2) (2007) 836–840, https://doi.org/10.1016/j.nimb.2007.02.078.
[24] D. Torresi, Excitation of Unbound States in 12B via the 8Li-alpha Resonant Elastic Scattering, PhD thesis, Universitá degli studi di Catania, Catania, Italy, 2011, http://www.infn.it/thesis/thesis$_$dettaglio.php$?$tid=6451.
[25] J. Ziegler, SRIM code, http://www.srim.org.
[26] A.M. Lane, R.G. Thomas, R-matrix theory of nuclear reactions, Rev. Mod. Phys. 30 (1958) 257–353, https://doi.org/10.1103/RevModPhys.30.257.
[27] R.E. Azuma, E. Uberseder, E.C. Simpson, C.R. Brune, H. Costantini, R.J. de Boer, J. Görres, M. Heil, P.J. LeBlanc, C. Ugalde, M. Wiescher, AZURE: an R-matrix code for nuclear astrophysics, Phys. Rev. C 81 (2010) 045805, https://doi.org/10.1103/PhysRevC.81.045805.

[28] NIST Digital Library of Mathematical Functions.
[29] P. Singh, P. Schwandt, G. Yang, Folding-model analysis of elastic alpha-nucleus scattering, Phys. Lett. B 59 (2) (1975) 113–117.
[30] J. Connor, New theoretical methods for molecular collisions: the complex angular-momentum approach, J. Chem. Soc. Faraday Trans. 86 (10) (1990) 1627–1640.
[31] R. Taylor, N. Fletcher, R. Davis, Elastic scattering of 4–20 MeV alpha particles by Be9, Nucl. Phys. 65 (2) (1965) 318–328, https://doi.org/10.1016/0029-5582(65)90272-5.
[32] I. Thompson, FRESCO code, http://www.fresco.org.uk.
[33] Low gas consumption fabrication of 3he solid targets for nuclear reactions, Mater. Des. 186 (2020) 108337, https://doi.org/10.1016/j.matdes.2019.108337.